DESY–07–062
11th May 2007

Multijet production at low x_{Bj} in deep inelastic scattering at HERA

ZEUS Collaboration

Abstract

Inclusive dijet and trijet production in deep inelastic ep scattering has been measured for $10 < Q^2 < 100$ GeV^2 and low Bjorken x, $10^{-4} < x_{\mathrm{Bj}} < 10^{-2}$. The data were taken at the HERA ep collider with centre-of-mass energy $\sqrt{s} = 318\,\mathrm{GeV}$ using the ZEUS detector and correspond to an integrated luminosity of 82 pb^{-1}. Jets were identified in the hadronic centre-of-mass (HCM) frame using the k_T cluster algorithm in the longitudinally invariant inclusive mode. Measurements of dijet and trijet differential cross sections are presented as functions of Q^2, x_{Bj}, jet transverse energy, and jet pseudorapidity. As a further examination of low-x_{Bj} dynamics, multi-differential cross sections as functions of the jet correlations in transverse momenta, azimuthal angles, and pseudorapidity are also presented. Calculations at $\mathcal{O}(\alpha_s^3)$ generally describe the trijet data well and improve the description of the dijet data compared to the calculation at $\mathcal{O}(\alpha_s^2)$.

The ZEUS Collaboration

S. Chekanov[1], M. Derrick, S. Magill, B. Musgrave, D. Nicholass[2], J. Repond, R. Yoshida
Argonne National Laboratory, Argonne, Illinois 60439-4815, USA [n]

M.C.K. Mattingly
Andrews University, Berrien Springs, Michigan 49104-0380, USA

M. Jechow, N. Pavel [†], A.G. Yagües Molina
Institut für Physik der Humboldt-Universität zu Berlin, Berlin, Germany

S. Antonelli, P. Antonioli, G. Bari, M. Basile, L. Bellagamba, M. Bindi, D. Boscherini, A. Bruni, G. Bruni, L. Cifarelli, F. Cindolo, A. Contin, M. Corradi[3], S. De Pasquale, G. Iacobucci, A. Margotti, R. Nania, A. Polini, G. Sartorelli, A. Zichichi
University and INFN Bologna, Bologna, Italy [e]

D. Bartsch, I. Brock, S. Goers[4], H. Hartmann, E. Hilger, H.-P. Jakob, M. Jüngst, O.M. Kind[5], A.E. Nuncio-Quiroz, E. Paul[6], R. Renner[4], U. Samson, V. Schönberg, R. Shehzadi, M. Wlasenko
Physikalisches Institut der Universität Bonn, Bonn, Germany [b]

N.H. Brook, G.P. Heath, J.D. Morris, T. Namsoo
H.H. Wills Physics Laboratory, University of Bristol, Bristol, United Kingdom [m]

M. Capua, S. Fazio, A. Mastroberardino, M. Schioppa, G. Susinno, E. Tassi
Calabria University, Physics Department and INFN, Cosenza, Italy [e]

J.Y. Kim[7], K.J. Ma[8]
Chonnam National University, Kwangju, South Korea [g]

Z.A. Ibrahim, B. Kamaluddin, W.A.T. Wan Abdullah
Jabatan Fizik, Universiti Malaya, 50603 Kuala Lumpur, Malaysia [r]

Y. Ning, Z. Ren, F. Sciulli
Nevis Laboratories, Columbia University, Irvington on Hudson, New York 10027 [o]

J. Chwastowski, A. Eskreys, J. Figiel, A. Galas, M. Gil, K. Olkiewicz, P. Stopa, L. Zawiejski
The Henryk Niewodniczanski Institute of Nuclear Physics, Polish Academy of Sciences, Cracow, Poland [i]

L. Adamczyk, T. Bołd, I. Grabowska-Bołd, D. Kisielewska, J. Łukasik, M. Przybycień, L. Suszycki
Faculty of Physics and Applied Computer Science, AGH-University of Science and Technology, Cracow, Poland [p]

A. Kotański[9], W. Słomiński[10]
Department of Physics, Jagellonian University, Cracow, Poland

V. Adler[11], U. Behrens, I. Bloch, C. Blohm, A. Bonato, K. Borras, R. Ciesielski, N. Coppola, A. Dossanov, V. Drugakov, J. Fourletova, A. Geiser, D. Gladkov, P. Göttlicher[12], J. Grebenyuk, I. Gregor, T. Haas, W. Hain, C. Horn[13], A. Hüttmann, B. Kahle, I.I. Katkov, U. Klein[14], U. Kötz, H. Kowalski, E. Lobodzinska, B. Löhr, R. Mankel, I.-A. Melzer-Pellmann, S. Miglioranzi, A. Montanari, D. Notz, L. Rinaldi, P. Roloff, I. Rubinsky, R. Santamarta, U. Schneekloth, A. Spiridonov[15], H. Stadie, D. Szuba[16], J. Szuba[17], T. Theedt, G. Wolf, K. Wrona, C. Youngman, W. Zeuner
Deutsches Elektronen-Synchrotron DESY, Hamburg, Germany

W. Lohmann, S. Schlenstedt
Deutsches Elektronen-Synchrotron DESY, Zeuthen, Germany

G. Barbagli, E. Gallo, P. G. Pelfer
University and INFN, Florence, Italy [e]

A. Bamberger, D. Dobur, F. Karstens, N.N. Vlasov[18]
Fakultät für Physik der Universität Freiburg i.Br., Freiburg i.Br., Germany [b]

P.J. Bussey, A.T. Doyle, W. Dunne, J. Ferrando, M. Forrest, D.H. Saxon, I.O. Skillicorn
Department of Physics and Astronomy, University of Glasgow, Glasgow, United Kingdom [m]

I. Gialas[19], K. Papageorgiu
Department of Engineering in Management and Finance, Univ. of Aegean, Greece

T. Gosau, U. Holm, R. Klanner, E. Lohrmann, H. Salehi, P. Schleper, T. Schörner-Sadenius, J. Sztuk, K. Wichmann, K. Wick
Hamburg University, Institute of Exp. Physics, Hamburg, Germany [b]

C. Foudas, C. Fry, K.R. Long, A.D. Tapper
Imperial College London, High Energy Nuclear Physics Group, London, United Kingdom [m]

M. Kataoka[20], T. Matsumoto, K. Nagano, K. Tokushuku[21], S. Yamada, Y. Yamazaki
Institute of Particle and Nuclear Studies, KEK, Tsukuba, Japan [f]

A.N. Barakbaev, E.G. Boos, N.S. Pokrovskiy, B.O. Zhautykov
Institute of Physics and Technology of Ministry of Education and Science of Kazakhstan, Almaty, Kazakhstan

V. Aushev[1]
Institute for Nuclear Research, National Academy of Sciences, Kiev and Kiev National University, Kiev, Ukraine

D. Son
Kyungpook National University, Center for High Energy Physics, Daegu, South Korea [g]

J. de Favereau, K. Piotrzkowski
Institut de Physique Nucléaire, Université Catholique de Louvain, Louvain-la-Neuve, Belgium [q]

F. Barreiro, C. Glasman[22], M. Jimenez, L. Labarga, J. del Peso, E. Ron, M. Soares, J. Terrón, M. Zambrana
Departamento de Física Teórica, Universidad Autónoma de Madrid, Madrid, Spain [l]

F. Corriveau, C. Liu, R. Walsh, C. Zhou
Department of Physics, McGill University, Montréal, Québec, Canada H3A 2T8 [a]

T. Tsurugai
Meiji Gakuin University, Faculty of General Education, Yokohama, Japan [f]

A. Antonov, B.A. Dolgoshein, V. Sosnovtsev, A. Stifutkin, S. Suchkov
Moscow Engineering Physics Institute, Moscow, Russia [j]

R.K. Dementiev, P.F. Ermolov, L.K. Gladilin, L.A. Khein, I.A. Korzhavina, V.A. Kuzmin, B.B. Levchenko[23], O.Yu. Lukina, A.S. Proskuryakov, L.M. Shcheglova, D.S. Zotkin, S.A. Zotkin
Moscow State University, Institute of Nuclear Physics, Moscow, Russia [k]

I. Abt, C. Büttner, A. Caldwell, D. Kollar, W.B. Schmidke, J. Sutiak
Max-Planck-Institut für Physik, München, Germany

G. Grigorescu, A. Keramidas, E. Koffeman, P. Kooijman, A. Pellegrino, H. Tiecke, M. Vázquez[20], L. Wiggers
NIKHEF and University of Amsterdam, Amsterdam, Netherlands [h]

N. Brümmer, B. Bylsma, L.S. Durkin, A. Lee, T.Y. Ling
Physics Department, Ohio State University, Columbus, Ohio 43210 [n]

P.D. Allfrey, M.A. Bell, A.M. Cooper-Sarkar, A. Cottrell, R.C.E. Devenish, B. Foster, K. Korcsak-Gorzo, S. Patel, V. Roberfroid[24], A. Robertson, P.B. Straub, C. Uribe-Estrada, R. Walczak
Department of Physics, University of Oxford, Oxford United Kingdom [m]

P. Bellan, A. Bertolin, R. Brugnera, R. Carlin, F. Dal Corso, S. Dusini, A. Garfagnini, S. Limentani, A. Longhin, L. Stanco, M. Turcato
Dipartimento di Fisica dell' Università and INFN, Padova, Italy [e]

B.Y. Oh, A. Raval, J. Ukleja[25], J.J. Whitmore[26]
Department of Physics, Pennsylvania State University, University Park, Pennsylvania 16802 [o]

Y. Iga
Polytechnic University, Sagamihara, Japan [f]

G. D'Agostini, G. Marini, A. Nigro
Dipartimento di Fisica, Università 'La Sapienza' and INFN, Rome, Italy [e]

J.E. Cole, J.C. Hart
Rutherford Appleton Laboratory, Chilton, Didcot, Oxon, United Kingdom [m]

H. Abramowicz[27], A. Gabareen, R. Ingbir, S. Kananov, A. Levy
Raymond and Beverly Sackler Faculty of Exact Sciences, School of Physics, Tel-Aviv University, Tel-Aviv, Israel [d]

M. Kuze, J. Maeda
Department of Physics, Tokyo Institute of Technology, Tokyo, Japan [f]

R. Hori, S. Kagawa[28], N. Okazaki, S. Shimizu, T. Tawara
Department of Physics, University of Tokyo, Tokyo, Japan [f]

R. Hamatsu, H. Kaji[29], S. Kitamura[30], O. Ota, Y.D. Ri
Tokyo Metropolitan University, Department of Physics, Tokyo, Japan [f]

M.I. Ferrero, V. Monaco, R. Sacchi, A. Solano
Università di Torino and INFN, Torino, Italy [e]

M. Arneodo, M. Ruspa
Università del Piemonte Orientale, Novara, and INFN, Torino, Italy [e]

S. Fourletov, J.F. Martin
Department of Physics, University of Toronto, Toronto, Ontario, Canada M5S 1A7 [a]

S.K. Boutle[19], J.M. Butterworth, C. Gwenlan[31], T.W. Jones, J.H. Loizides, M.R. Sutton[31], M. Wing
Physics and Astronomy Department, University College London, London, United Kingdom [m]

B. Brzozowska, J. Ciborowski[32], G. Grzelak, P. Kulinski, P. Łużniak[33], J. Malka[33], R.J. Nowak, J.M. Pawlak, T. Tymieniecka, A. Ukleja, A.F. Żarnecki
Warsaw University, Institute of Experimental Physics, Warsaw, Poland

M. Adamus, P. Plucinski[34]
Institute for Nuclear Studies, Warsaw, Poland

Y. Eisenberg, I. Giller, D. Hochman, U. Karshon, M. Rosin
Department of Particle Physics, Weizmann Institute, Rehovot, Israel [c]

E. Brownson, T. Danielson, A. Everett, D. Kçira, D.D. Reeder[6], P. Ryan, A.A. Savin, W.H. Smith, H. Wolfe
Department of Physics, University of Wisconsin, Madison, Wisconsin 53706, USA [n]

S. Bhadra, C.D. Catterall, Y. Cui, G. Hartner, S. Menary, U. Noor, J. Standage, J. Whyte
Department of Physics, York University, Ontario, Canada M3J 1P3 [a]

[1] supported by DESY, Germany
[2] also affiliated with University College London, UK
[3] also at University of Hamburg, Germany, Alexander von Humboldt Fellow
[4] self-employed
[5] now at Humboldt University, Berlin, Germany
[6] retired
[7] supported by Chonnam National University in 2005
[8] supported by a scholarship of the World Laboratory Björn Wiik Research Project
[9] supported by the research grant no. 1 P03B 04529 (2005-2008)
[10] This work was supported in part by the Marie Curie Actions Transfer of Knowledge project COCOS (contract MTKD-CT-2004-517186)
[11] now at Univ. Libre de Bruxelles, Belgium
[12] now at DESY group FEB, Hamburg, Germany
[13] now at Stanford Linear Accelerator Center, Stanford, USA
[14] now at University of Liverpool, UK
[15] also at Institut of Theoretical and Experimental Physics, Moscow, Russia
[16] also at INP, Cracow, Poland
[17] on leave of absence from FPACS, AGH-UST, Cracow, Poland
[18] partly supported by Moscow State University, Russia
[19] also affiliated with DESY
[20] now at CERN, Geneva, Switzerland
[21] also at University of Tokyo, Japan
[22] Ramón y Cajal Fellow
[23] partly supported by Russian Foundation for Basic Research grant no. 05-02-39028-NSFC-a
[24] EU Marie Curie Fellow
[25] partially supported by Warsaw University, Poland
[26] This material was based on work supported by the National Science Foundation, while working at the Foundation.
[27] also at Max Planck Institute, Munich, Germany, Alexander von Humboldt Research Award
[28] now at KEK, Tsukuba, Japan
[29] now at Nagoya University, Japan
[30] Department of Radiological Science
[31] PPARC Advanced fellow
[32] also at Łódź University, Poland
[33] Łódź University, Poland
[34] supported by the Polish Ministry for Education and Science grant no. 1 P03B 14129
[†] deceased

[a] supported by the Natural Sciences and Engineering Research Council of Canada (NSERC)

[b] supported by the German Federal Ministry for Education and Research (BMBF), under contract numbers HZ1GUA 2, HZ1GUB 0, HZ1PDA 5, HZ1VFA 5

[c] supported in part by the MINERVA Gesellschaft für Forschung GmbH, the Israel Science Foundation (grant no. 293/02-11.2) and the U.S.-Israel Binational Science Foundation

[d] supported by the German-Israeli Foundation and the Israel Science Foundation

[e] supported by the Italian National Institute for Nuclear Physics (INFN)

[f] supported by the Japanese Ministry of Education, Culture, Sports, Science and Technology (MEXT) and its grants for Scientific Research

[g] supported by the Korean Ministry of Education and Korea Science and Engineering Foundation

[h] supported by the Netherlands Foundation for Research on Matter (FOM)

[i] supported by the Polish State Committee for Scientific Research, grant no. 620/E-77/SPB/DESY/P-03/DZ 117/2003-2005 and grant no. 1P03B07427/2004-2006

[j] partially supported by the German Federal Ministry for Education and Research (BMBF)

[k] supported by RF Presidential grant N 8122.2006.2 for the leading scientific schools and by the Russian Ministry of Education and Science through its grant Research on High Energy Physics

[l] supported by the Spanish Ministry of Education and Science through funds provided by CICYT

[m] supported by the Particle Physics and Astronomy Research Council, UK

[n] supported by the US Department of Energy

[o] supported by the US National Science Foundation. Any opinion, findings and conclusions or recommendations expressed in this material are those of the authors and do not necessarily reflect the views of the National Science Foundation.

[p] supported by the Polish Ministry of Science and Higher Education as a scientific project (2006-2008)

[q] supported by FNRS and its associated funds (IISN and FRIA) and by an Inter-University Attraction Poles Programme subsidised by the Belgian Federal Science Policy Office

[r] supported by the Malaysian Ministry of Science, Technology and Innovation/Akademi Sains Malaysia grant SAGA 66-02-03-0048

1 Introduction

Multijet production in deep inelastic ep scattering (DIS) at HERA has been used to test the predictions of perturbative QCD (pQCD) over a large range of negative four-momentum transfer squared, Q^2, and to determine the strong coupling constant α_s [1,2]. At leading order (LO) in α_s, dijet production in neutral current DIS proceeds via the boson-gluon-fusion ($V^*g \to q\bar{q}$ with $V = \gamma, Z^0$) and QCD-Compton ($V^*q \to qg$) processes. Events with three jets can be seen as dijet processes with an additional gluon radiation or with a gluon splitting into a quark-antiquark pair and are directly sensitive to $\mathcal{O}(\alpha_s^2)$ QCD effects. The higher sensitivity to α_s and the large number of degrees of freedom of the trijet final state provide a good testing ground for the pQCD predictions. In particular, multijet production in DIS is an ideal environment for investigating different approaches to parton dynamics at low Bjorken-x, x_{Bj} [3]. An understanding of this regime is of particular relevance in view of the startup of the LHC, where many of the Standard Model processes such as the production of electroweak gauge bosons or the Higgs particle involve the collision of partons with a low fraction of the proton momentum.

In the usual collinear QCD factorisation approach, the cross sections are obtained as the convolution of perturbative matrix elements and parton densities evolved according to the DGLAP evolution equations [4]. These equations resum to all orders the terms proportional to $\alpha_s \ln Q^2$ and the double logarithms $\ln Q^2 \cdot \ln 1/x$, where x is the fraction of the proton momentum carried by a parton, which is equal to x_{Bj} in the quark-parton model. In the DGLAP approach, the parton participating in the hard scattering is the result of a partonic cascade ordered in transverse momentum, p_T. The partonic cascade starts from a low-p_T and high-x parton from the incoming proton and ends up, after consecutive branching, in the high-p_T and low-x parton entering in the hard scattering. This approximation has been tested extensively at HERA and was found to describe well the inclusive cross sections [5,6] and jet production [1,2,7,8]. At low x_{Bj}, where the phase space for parton emissions increases, terms proportional to $\alpha_s \ln 1/x$ may become large and spoil the accuracy of the DGLAP approach. In this region the transverse momenta and angular correlations between partons produced in the hard scatter may be sensitive to effects beyond DGLAP dynamics. The information about cross sections, transverse energy, E_T, and angular correlations between the two leading jets in multijet production therefore provides an important testing ground for studying the parton dynamics in the region of small x_{Bj}.

In this analysis, correlations for both azimuthal and polar angles, and correlations in jet transverse energy and momenta for dijet and trijet production in the hadronic ($\gamma^* p$) centre-of-mass (HCM) frame are measured with high statistical precision in the kinematic region restricted to $10 < Q^2 < 100\,\mathrm{GeV}^2$ and $10^{-4} < x_{\mathrm{Bj}} < 10^{-2}$. The results are compared

with pQCD calculations at next-to-leading order (NLO). A similar study of inclusive dijet production was performed by the H1 collaboration [9].

2 Experimental set-up

The data used in this analysis were collected during the 1998-2000 running period, when HERA operated with protons of energy $E_p = 920$ GeV and electrons or positrons[1] of energy $E_e = 27.5$ GeV, and correspond to an integrated luminosity of 81.7 ± 1.8 pb^{-1}. A detailed description of the ZEUS detector can be found elsewhere [10, 11]. A brief outline of the components that are most relevant for this analysis is given below.

Charged particles are measured in the central tracking detector (CTD) [12], which operates in a magnetic field of 1.43 T provided by a thin superconducting solenoid. The CTD consists of 72 cylindrical drift chamber layers, organised in nine superlayers covering the polar-angle[2] region $15^\circ < \theta < 164^\circ$. The transverse momentum resolution for full-length tracks can be parameterised as $\sigma(p_T)/p_T = 0.0058 p_T \oplus 0.0065 \oplus 0.0014/p_T$, with p_T in GeV. The tracking system was used to measure the interaction vertex with a typical resolution along (transverse to) the beam direction of 0.4 (0.1) cm and also to cross-check the energy scale of the calorimeter.

The high-resolution uranium-scintillator calorimeter (CAL) [13] covers 99.7% of the total solid angle and consists of three parts: the forward (FCAL), the barrel (BCAL) and the rear (RCAL) calorimeters. Each part is subdivided transversely into towers and longitudinally into one electromagnetic section and either one (in RCAL) or two (in BCAL and FCAL) hadronic sections. The smallest subdivision of the calorimeter is called a cell. Under test-beam conditions, the CAL single-particle relative energy resolutions were $\sigma(E)/E = 0.18/\sqrt{E}$ for electrons and $\sigma(E)/E = 0.35/\sqrt{E}$ for hadrons, with E in GeV.

The luminosity was measured from the rate of the bremsstrahlung process $ep \to e\gamma p$. The resulting small-angle energetic photons were measured by the luminosity monitor [14], a lead-scintillator calorimeter placed in the HERA tunnel at $Z = -107$ m.

[1] In the following, the term "electron" denotes generically both the electron (e^-) and the positron (e^+).
[2] The ZEUS coordinate system is a right-handed Cartesian system, with the Z axis pointing in the proton beam direction, referred to as the "forward direction", and the X axis pointing left towards the centre of HERA. The coordinate origin is at the nominal interaction point.

3 Kinematics and event selection

A three-level trigger system was used to select events online [11, 15]. Neutral current DIS events were selected by requiring that a scattered electron candidate with an energy more than 4 GeV was measured in the CAL. The variable $x_{\rm Bj}$, the inelasticity y, and Q^2 were reconstructed offline using the electron (subscript e) [16] and Jacquet-Blondel (JB) [17] methods. For each event, the reconstruction of the hadronic final state was performed using a combination of track and CAL information, excluding the cells and the track associated with the scattered electron. The selected tracks and CAL clusters were treated as massless energy flow objects (EFOs) [18].

The offline selection of DIS events was similar to that used in the previous ZEUS measurement [1] and was based on the following requirements:

- $E'_e > 10\,\text{GeV}$, where E'_e is the scattered electron energy after correction for energy loss from the inactive material in the detector;
- $y_e < 0.6$ and $y_{\rm JB} > 0.1$, to ensure a kinematic region with good reconstruction;
- $40 < \delta < 60\,\text{GeV}$, where $\delta = \sum_i (E_i - P_{Z,i})$, where E_i and $P_{Z,i}$ are the energy and z-momentum of each final-state object. The lower cut removed background from photoproduction and events with large initial-state QED radiation, while the upper cut removed cosmic-ray background;
- $|Z_{\rm vtx}| < 50$ cm, where $Z_{\rm vtx}$ is the Z position of the reconstructed primary vertex, to select events consistent with ep collisions.

The kinematic range of the analysis is

$$10 < Q^2 < 100\,\text{GeV}^2,\ 10^{-4} < x_{\rm Bj} < 10^{-2} \text{ and } 0.1 < y < 0.6.$$

Jets were reconstructed using the k_T cluster algorithm [19] in the longitudinally invariant inclusive mode [20]. The jet search was conducted in the HCM frame, which is equivalent to the Breit frame [21] apart from a longitudinal boost.

The jet phase space is defined by selection cuts on the jet pseudorapidity, $\eta^{\rm jet}_{\rm LAB}$, in the laboratory frame and on the jet transverse energy, $E^{\rm jet}_{T,\rm HCM}$, in the HCM frame:

$$-1.0 < \eta^{\rm jet1,2(,3)}_{\rm LAB} < 2.5 \text{ and } E^{\rm jet1}_{T,\rm HCM} > 7 \text{ GeV}, E^{\rm jet2(,3)}_{T,\rm HCM} > 5 \text{ GeV},$$

where jet1,2(,3) refers to the two (three) jets with the highest transverse energy in the HCM frame for a given event. The dijet and trijet samples are inclusive in that they contain at least two or three jets passing the selection criteria, respectively.

4 Monte Carlo simulation

Monte Carlo (MC) simulations were used to correct the data for detector effects, inefficiencies of the event selection and the jet reconstruction, as well as for QED effects. Neutral current DIS events were generated using the ARIADNE 4.10 program [22] and the LEPTO 6.5 program [23] interfaced to HERACLES 4.5.2 [24] via DJANGO 6.2.4 [25]. The HERACLES program includes QED effects up to $\mathcal{O}(\alpha_{\rm EM}^2)$. In the case of ARIADNE, events were generated using the colour-dipole model [26], whereas for LEPTO, the matrix-elements plus parton-shower model was used. The CTEQ5L parameterisations of the proton parton density functions (PDFs) [27] were used in the generation of DIS events for ARIADNE, and the CTEQ4D PDFs [27] were used for LEPTO. For hadronisation the Lund string model [28], as implemented in JETSET 7.4 [29, 30] was used.

The ZEUS detector response was simulated with a program based on GEANT 3.13 [31]. The generated events were passed through the detector simulation, subjected to the same trigger requirements as the data, and processed by the same reconstruction and offline programs.

The measured distributions of the global kinematic variables are well described by both the ARIADNE and LEPTO MC models after reweighting in Q^2 [1]. The LEPTO simulation gives a better overall description of the jet variables, but ARIADNE provides a better description of dijets with small azimuthal separation. Therefore, for this analysis, the events generated with the ARIADNE program were used to determine the acceptance corrections. The events generated with LEPTO were used to estimate the uncertainty associated with the treatment of the parton shower.

5 NLO QCD calculations

The NLO calculations were carried out in the $\overline{\rm MS}$ scheme for five massless quark flavors with the program NLOJET [32]. The NLOJET program allows a computation of the dijet (trijet) production cross sections to next-to-leading order, i.e. including all terms up to $\mathcal{O}(\alpha_s^2)$ ($\mathcal{O}(\alpha_s^3)$). In certain regions of the jet phase space, where the two hardest jets are not balanced in transverse momentum, NLOJET can be used to calculate the cross sections for dijet production at $\mathcal{O}(\alpha_s^3)$. It was checked that the LO and NLO calculations from NLOJET agree with those of DISENT [33] at the 1-2% level for the dijet cross sections [34, 35].

For comparison with the data, the CTEQ6M [36] PDFs were used, and the renormalisation and factorisation scales were both chosen to be $(\bar{E}_{T,\rm HCM}^2 + Q^2)/4$, where for dijets (trijets) $\bar{E}_{T,\rm HCM}$ is the average $E_{T,\rm HCM}$ of the two (three) highest $E_{T,\rm HCM}$ jets in a given event.

The choice of renormalisation scale matches that used in the previous ZEUS multijet analysis [1]. The strong coupling constant was set to the value used for the CTEQ6 PDFs, $\alpha_s(M_Z) = 0.118$, and evolved according to the two-loop solution of the renormalisation group equation.

The NLO QCD predictions were corrected for hadronisation effects using a bin-by-bin procedure. Hadronisation correction factors were defined for each bin as the ratio of the hadron- to parton-level cross sections and were calculated using the LEPTO MC program, which, at the parton level, gives a better agreement with NLOJET than ARIADNE. The correction factors $C_{\rm had}$ were typically in the range $0.8 - 0.9$ for most of the phase space.

The theoretical uncertainty was estimated by varying the renormalisation scale up and down by a factor of two. The uncertainties in the proton PDFs were estimated in the previous ZEUS multijets analysis [1] by repeating NLOJET calculations using 40 additional sets from CTEQ6M, which resulted in a 2.5% contribution to the theoretical uncertainty and was therefore neglected.

6 Acceptance Corrections

The ARIADNE MC was used to correct the data for detector effects. The jet transverse energies were corrected for energy losses from inactive material in the detector. Typical jet energy correction factors were $1 - 1.2$, depending on the transverse energy of the detector-level jet and the jet pseudorapidity.

The measured cross sections were corrected to the hadron level using a bin-by-bin procedure. These corrections account for trigger efficiency, acceptance, and migration. Typical efficiencies and purities were about 50% for the differential cross sections, with correction factors typically between 1 and 1.5. For the double-differential cross sections, the efficiencies and purities were typically $20 - 50\%$, with correction factors between 1 and 2.

The cross sections were corrected to the QED Born level by applying an additional correction obtained from a special sample of the LEPTO MC with the radiative QED effects turned off. The QED radiative effects were typically $2 - 4\%$.

7 Systematic uncertainties

A detailed study of the sources contributing to the systematic uncertainties of the measurements has been performed. The main sources contributing to the systematic uncertainties are listed below:

- the data were corrected using LEPTO instead of ARIADNE;
- the jet energies in the data were scaled up and down by 3% for jets with transverse energy less than 10 GeV and 1% for jets with transverse energy above 10 GeV, according to the estimated jet energy scale uncertainty [37];
- the cut on $E_{T,\mathrm{HCM}}^{\mathrm{jet}}$ for each jet was raised and lowered by 1 GeV, corresponding to the E_T resolution;
- the upper and lower cuts on $\eta_{\mathrm{LAB}}^{\mathrm{jet1,2(,3)}}$ were each changed by ± 0.1, corresponding to the η resolution;
- the uncertainties due to the selection cuts was estimated by varying the cuts within the resolution of each variable.

The largest systematic uncertainties came from the uncertainty of the jet energy scale, which produced a systematic uncertainty of $5-10\%$. For the trijet sample, altering the cut on $E_{T,\mathrm{HCM}}^{\mathrm{et3}}$ also produced a systematic uncertainty of $5-10\%$. The other significant systematic uncertainty arose from the choice of LEPTO instead of ARIADNE for correcting detector effects. This systematic uncertainty was also typically $5-10\%$. The other systematic uncertainties were smaller than or similar to the statistical uncertainties.

The systematic uncertainties not associated with the absolute energy scale of the jets were added in quadrature to the statistical uncertainties and are shown as error bars in the figures. The uncertainty due to the absolute energy scale of the jets is shown separately as a shaded band in each figure, due to the large bin-to-bin correlation. In addition, there is an overall normalisation uncertainty of 2.2% from the luminosity determination, which is not included in the figures.

8 Results

8.1 Single-differential cross sections $d\sigma/dQ^2$, $d\sigma/dx_{\mathrm{Bj}}$ and trijet to dijet cross section ratios

The single-differential cross-sections $d\sigma/dQ^2$ and $d\sigma/dx_{\mathrm{Bj}}$ for dijet and trijet production are presented in Figs. 1(a) and (c), and Tables 1 – 4. The ratio $\sigma_{\mathrm{trijet}}/\sigma_{\mathrm{dijet}}$ of the trijet cross section to the dijet cross section, as a function of Q^2 and of x_{Bj} are presented in Figs. 1(b) and 1(d), respectively. The ratio $\sigma_{\mathrm{trijet}}/\sigma_{\mathrm{dijet}}$ is almost Q^2 independent, as shown in Fig. 1(b), and falls steeply with increasing x_{Bj}, as shown in Fig. 1(d). In the cross-section ratios, the experimental and theoretical uncertainties partially cancel, providing a possibility to test the pQCD calculations more precisely than can be done

with the individual cross sections. Both the cross sections and the cross-section ratios are well described by the NLOJET calculations.

8.2 Transverse energy and pseudorapidity dependencies of cross sections

The single-differential cross-sections $d\sigma/dE^{\mathrm{jet}}_{T,\mathrm{HCM}}$ for two (three) jet events are presented in Fig. 2. The measured cross sections are well described by the NLOJET calculations over the whole range in $E^{\mathrm{jet}}_{T,\mathrm{HCM}}$ considered.

The single-differential cross sections $d\sigma/d\eta^{\mathrm{jet}}_{\mathrm{LAB}}$ for dijet and trijet production are presented in Figs. 3(a) and 3(c). For this figure, the two (three) jets with highest $E^{\mathrm{jet}}_{T,\mathrm{HCM}}$ were ordered in $\eta^{\mathrm{jet}}_{\mathrm{LAB}}$. Also shown are the measurements of the single-differential cross-sections $d\sigma/d|\Delta\eta^{\mathrm{jet1,2}}_{\mathrm{HCM}}|$, where $|\Delta\eta^{\mathrm{jet1,2}}_{\mathrm{HCM}}|$ is the absolute difference in pseudorapidity of the two jets with highest $E^{\mathrm{jet}}_{T,\mathrm{HCM}}$ (see Figs. 3(b) and 3(d)). The NLOJET predictions describe the measurements well.

8.3 Jet transverse energy and momentum correlations

Correlations in transverse energy of the jets have been investigated by measuring the double-differential cross-sections $d^2\sigma/dx_{\mathrm{Bj}}d\Delta E^{\mathrm{jet1,2}}_{T,\mathrm{HCM}}$, where $\Delta E^{\mathrm{jet1,2}}_{T,\mathrm{HCM}}$ is the difference in transverse energy between the two jets with the highest $E^{\mathrm{jet}}_{T,\mathrm{HCM}}$. The measurement was performed in x_{Bj} bins, which are defined in Table 2, for dijet and trijet production. Figures 4 and 5 show the cross-sections $d^2\sigma/dx_{\mathrm{Bj}}d\Delta E^{\mathrm{jet1,2}}_{T,\mathrm{HCM}}$ for all bins in x_{Bj} for the dijet and trijet samples, respectively.

The NLOJET calculations at $\mathcal{O}(\alpha_s^2)$ do not describe the high-$\Delta E^{\mathrm{jet1,2}}_{T,\mathrm{HCM}}$ tail of the dijet sample at low x_{Bj}, where the calculations fall below the data. Since these calculations give the lowest-order non-trivial contribution to the cross section in the region $\Delta E^{\mathrm{jet1,2}}_{T,\mathrm{HCM}} > 0$, they are affected by large uncertainties from the higher-order terms in α_s. A higher-order calculation for the dijet sample is possible with NLOJET if the region $\Delta E^{\mathrm{jet1,2}}_{T,\mathrm{HCM}}$ near zero is avoided. NLOJET calculations at $\mathcal{O}(\alpha_s^3)$ for the dijet sample have been obtained for the region $\Delta E^{\mathrm{jet1,2}}_{T,\mathrm{HCM}} > 4\,\mathrm{GeV}$ and are compared to the data in Fig. 4. With the inclusion of the next term in the perturbative series in α_s, the NLOJET calculations describe the data within the theoretical uncertainties. The NLOJET calculations at $\mathcal{O}(\alpha_s^3)$ for trijet production are consistent with the measurements.

As a refinement to the studies of the correlations between the transverse energies of the jets, further correlations of the jet tranverse momenta have been investigated. The correlations in jet transverse momenta were examined by measuring two sets of double-differential

cross sections: $d^2\sigma/dx_{\rm Bj}d|\Sigma\vec{p}^{\,\rm jet1,2}_{T,\rm HCM}|$ and $d^2\sigma/dx_{\rm Bj}d(|\Delta\vec{p}^{\,\rm jet1,2}_{T,\rm HCM}|/(2E^{\rm jet1}_{T,\rm HCM}))$. The variable $|\Sigma\vec{p}^{\,\rm jet1,2}_{T,\rm HCM}|$ is the transverse component of the vector sum of the jet momenta of the two jets with the highest $E^{\rm jet}_{T,\rm HCM}$. For events with only two jets $|\Sigma\vec{p}^{\,\rm jet1,2}_{T,\rm HCM}| = 0$, and additional QCD radiation increases this value. The variable $|\Delta\vec{p}^{\,\rm jet1,2}_{T,\rm HCM}|/(2E^{\rm jet1}_{T,\rm HCM})$ is the magnitude of the vector difference of the transverse momenta of the two jets with the highest $E^{\rm jet}_{T,\rm HCM}$ scaled by twice the transverse energy of the hardest jet. For events with only two jets $|\Delta\vec{p}^{\,\rm jet1,2}_{T,\rm HCM}|/(2E^{\rm jet1}_{T,\rm HCM}) = 1$, and additional QCD radiation decreases this value. Figures 6 – 9 show the cross-sections $d^2\sigma/dx_{\rm Bj}d|\Sigma\vec{p}^{\,\rm jet1,2}_{T,\rm HCM}|$ and the cross-sections $d^2\sigma/dx_{\rm Bj}d|\Delta\vec{p}^{\,\rm jet1,2}_{T,\rm HCM}|/(2E^{\rm jet1}_{T,\rm HCM})$ in bins of $x_{\rm Bj}$ for the dijet and trijet samples.

At low $x_{\rm Bj}$, the NLOJET calculations at $\mathcal{O}(\alpha_s^2)$ underestimate the dijet cross sections at high values of $|\Sigma\vec{p}^{\,\rm jet1,2}_{T,\rm HCM}|$ and low values of $|\Delta\vec{p}^{\,\rm jet1,2}_{T,\rm HCM}|/(2E^{\rm jet1}_{T,\rm HCM})$. The description of the data by the NLOJET calculations at $\mathcal{O}(\alpha_s^2)$ improves at higher values of $x_{\rm Bj}$. A higher-order calculation with NLOJET at $\mathcal{O}(\alpha_s^3)$ for the dijet sample has been obtained for the region $|\Sigma\vec{p}^{\,\rm jet1,2}_{T,\rm HCM}| > 4\,\text{GeV}$, which is compared to the data in Fig. 6; and for the region $|\Delta\vec{p}^{\,\rm jet1,2}_{T,\rm HCM}|/(2E^{\rm jet1}_{T,\rm HCM}) < 0.85$, which is compared to the data in Fig. 8. With the inclusion of the next term in the perturbative series in α_s, the NLOJET calculations describe the data well. The NLOJET calculations at $\mathcal{O}(\alpha_s^3)$ for trijet production are consistent with the measurements.

8.4 Azimuthal distributions of the jets

Measurements of the double-differential cross-section $d^2\sigma/dx_{\rm Bj}d|\Delta\phi^{\rm jet1,2}_{\rm HCM}|$, where $|\Delta\phi^{\rm jet1,2}_{\rm HCM}|$ is the azimuthal separation of the two jets with the largest $E^{\rm jet}_{T,\rm HCM}$, for dijet and trijet production are shown in Figs. 10 and 11 for all bins in $x_{\rm Bj}$. For both dijet and trijet production the cross section falls with $|\Delta\phi^{\rm jet1,2}_{\rm HCM}|$. The NLOJET calculations at $\mathcal{O}(\alpha_S^2)$ for dijet production decrease more rapidly with $|\Delta\phi^{\rm jet1,2}_{\rm HCM}|$ than the data and the calculations disagree with the data at low $|\Delta\phi^{\rm jet1,2}_{\rm HCM}|$. A higher-order NLOJET calculation at $\mathcal{O}(\alpha_S^3)$ for the dijet sample has been obtained for the region $|\Delta\phi^{\rm jet1,2}_{\rm HCM}| < 3\pi/4$ and describes the data well. The measurements for trijet production are reasonably well described by the NLOJET calculations at $\mathcal{O}(\alpha_S^3)$.

A further investigation has been performed by measuring the cross-section $d^2\sigma/dQ^2dx_{\rm Bj}$ for dijet (trijet) events with $|\Delta\phi^{\rm jet1,2}_{\rm HCM}| < 2\pi/3$ as a function of $x_{\rm Bj}$. For the two-jet final states, the presence of two leading jets with $|\Delta\phi^{\rm jet1,2}_{\rm HCM}| < 2\pi/3$ can indicate another high-E_T jet or set of high-E_T jets outside the measured η range. These cross sections are presented in Fig. 12. The NLOJET calculations at $\mathcal{O}(\alpha_S^2)$ for dijet production underestimate the data, the difference increasing towards low $x_{\rm Bj}$. The NLOJET calculations at $\mathcal{O}(\alpha_S^3)$ are up to about one order of magnitude larger than the $\mathcal{O}(\alpha_S^2)$ calculations and are consistent with the data, demonstrating the importance of the higher-order terms in the description

of the data especially at low x_{Bj}. The NLOJET calculations at $\mathcal{O}(\alpha_S^3)$ describe the trijet data within the renormalisation-scale uncertainties.

9 Summary

Dijet and trijet production in deep inelastic ep scattering has been measured in the phase space region $10 < Q^2 < 100$ GeV^2 and $10^{-4} < x_{\mathrm{Bj}} < 10^{-2}$ using an integrated luminosity of 82 pb^{-1} collected by the ZEUS experiment. The high statistics have made possible detailed studies of multijet production at low x_{Bj}. The dependence of dijet and trijet production on the kinematic variables Q^2 and x_{Bj} and on the jet variables $E_{T,\mathrm{HCM}}^{\mathrm{jet}}$ and $\eta_{\mathrm{LAB}}^{\mathrm{jet}}$ is well described by perturbative QCD calculations which include NLO corrections. To investigate possible deviations with respect to the collinear factorisation approximation used in the standard pQCD approach, measurements of the correlations between the two jets with highest $E_{T,\mathrm{HCM}}^{\mathrm{jet}}$ have been made. At low x_{Bj}, measurements of dijet production with low azimuthal separation are reproduced by the perturbative QCD calculations provided that higher-order terms ($\mathcal{O}(\alpha_s^3)$) are accounted for. Such terms increase the predictions of pQCD calculations by up to one order of magnitude when the two jets with the highest $E_{T,\mathrm{HCM}}^{\mathrm{jet1,2}}$ are not balanced in transverse momentum. This demonstrates the importance of higher-order corrections in the low-x_{Bj} region.

Acknowledgements

It is a pleasure to thank the DESY Directorate for their strong support and encouragement. The remarkable achievements of the HERA machine group were essential for the successful completion of this work and are greatly appreciated. The design, construction and installation of the ZEUS detector has been made possible by the efforts of many people who are not listed as authors. It is also a pleasure to thank Zoltan Nagy for useful discussions about NLOJET.

References

[1] ZEUS Coll., S. Chekanov et al., Eur. Phys. J. C 44 (2005) 183.

[2] H1 Coll., Adloff, C. et al., Phys. Lett. B515 (2001) 17.

[3] J.D. Bjorken, Phys. Rev. 179 (1969) 1547.

[4] V.N. Gribov and L.N. Lipatov, Sov. J. Nucl. Phys. 15 (1972) 438;
G. Altarelli and G. Parisi, Nucl. Phys. B 126 (1977) 298;
L.N. Lipatov, Sov. J. Nucl. Phys. 20 (1975) 94;
Yu.L. Dokshitzer, Sov. Phys. JETP 46 (1977) 641.

[5] H1 Coll., C. Adloff et al., Eur. Phys. J. C 21 (2001) 33.

[6] ZEUS Coll., S. Chekanov et al., Phys. Rev. D 67 (2003) 012007.

[7] ZEUS Coll., S. Chekanov et al., Eur. Phys. J. C 23 (2002) 13;
ZEUS Coll., S. Chekanov et al., Phys. Lett. B 547 (2002) 164;
ZEUS Coll., S. Chekanov et al., Eur. Phys. J. C 21 (2001) 443.

[8] H1 Coll., C. Adloff et al., Eur. Phys. J. C 19 (2001) 289;
H1 Coll., C. Adloff et al., Phys. Lett. B 515 (2001) 17;
H1 Coll., S. Aid et al., Nucl. Phys. B 470 (1996) 3.

[9] H1 Coll., A. Aktas et al., Eur. Phys. J. C 33 (2004) 477.

[10] ZEUS Coll., M. Derrick et al., Phys. Lett. B 293 (1992) 465.

[11] ZEUS Coll., U. Holm (ed.), *The ZEUS Detector*. Status Report (unpublished), DESY (1993), available on `http://www-zeus.desy.de/bluebook/bluebook.html`.

[12] N. Harnew et al., Nucl. Instr. Meth. A 279 (1989) 290;
B. Foster et al., Nucl. Phys. Proc. Suppl. B 32 (1993) 181;
B. Foster et al., Nucl. Instr. Meth. A 338 (1994) 254.

[13] M. Derrick et al., Nucl. Instr. Meth. A 309 (1991) 77;
A. Andresen et al., Nucl. Instr. Meth. A 309 (1991) 101;
A. Caldwell et al., Nucl. Instr. Meth. A 321 (1992) 356;
A. Bernstein et al., Nucl. Instr. Meth. A 336 (1993) 23.

[14] J. Andruszków et al., Preprint DESY-92-066, DESY, 1992;
ZEUS Coll., M. Derrick et al., Z. Phys. C 63 (1994) 391;
J. Andruszków et al., Acta Phys. Pol. B 32 (2001) 2025.

[15] W.H. Smith, K. Tokushuku and L.W. Wiggers, *Proceedings of the Computing in High Energy Physics (CHEP 92)*, C. Verkerk and W. Wojcik (eds.), p. 222. Geneva, Switzerland (1992). Also in preprint DESY 92-150B.

[16] K.C. Höger, *Proc. Workshop on Physics at HERA*, W. Buchmüller and G. Ingelman (eds.), Vol. 1, p. 43. Hamburg, Germany, DESY (1992).

[17] F. Jacquet and A. Blondel, *Proceedings of the Study for an ep Facility for Europe*, U. Amaldi (ed.), p. 391. Hamburg, Germany (1979). Also in preprint DESY 79/48.

[18] G.M. Briskin. Ph.D. Thesis, Tel Aviv University, 1998. DESY-THESIS-1998-036.

[19] S. Catani et al., Nucl. Phys. B 406 (1993) 187.

[20] S.D. Ellis and D.E. Soper, Phys. Rev. D 48 (1993) 3160.

[21] R.P. Feynman, *Photon-Hadron Interactions*. Benjamin, New York, 1972; K.H. Streng, T.F. Walsh, P.M. Zerwas, Z. Phys. C (1979) 237.

[22] L. Lönnblad, Comput. Phys. Comm. 71 (1992) 15.

[23] G. Ingelman, A. Edin and J. Rathsman, Comput. Phys. Comm. 101 (1997) 108.

[24] A. Kwiatkowski, H. Spiesberger and H.-J. Möhring, Comput. Phys. Comm. 69 (1992) 155. Also in *Proc. Workshop Physics at HERA*, 1991, DESY, Hamburg.

[25] K. Charchula, G.A. Schuler and H. Spiesberger, Comput. Phys. Comm. 81 (1994) 381.

[26] G. Gustafson and U. Pettersson, Nucl. Phys. B 306 (1988) 746.

[27] H.L. Lai et al., Phys. Rev. D 55 (1997) 1280.

[28] B. Andersson et al., Phys. Rep. 97 (1983) 31.

[29] M. Bengtsson and T. Sjöstrand, Comput. Phys. Comm. 46 (1987) 43.

[30] T. Sjöstrand, Comput. Phys. Comm. 82 (1994) 74.

[31] R. Brun et al., GEANT3, Technical Report CERN-DD/EE/84-1, CERN, 1987.

[32] Z. Nagy and Z Trocsanyi, Phys. Rev. Lett. 87 (2001) 082001.

[33] S. Catani and M. H. Seymour, Nucl. Phys. B 485 (1997) 291.

[34] N. Krumnack. Ph.D. Thesis, University of Hamburg, 2004.

[35] L. Li. Ph.D. Thesis, University of Wisconsin-Madison, 2004.

[36] J. Pumplin et al., JHEP 07 (2002) 012.

[37] ZEUS Coll., S. Chekanov et al., Eur. Phys. J. C 27 (2003) 531; ZEUS Coll., S. Chekanov et al., Eur. Phys. J. C 23 (2002) 615; Wing, M. (on behalf of the ZEUS Coll.). Proc. of the 10th International Conference on Calorimetry in High Energy Physics, R. Zhu (ed.), p. 767. Pasadena, USA (2002). Also in preprint hep-ex/0206036.

[38] T. Gosau. Ph.D. Thesis, University of Hamburg, 2007. In preparation.

[39] T. Danielson. Ph.D. Thesis, University of Wisconsin - Madison, 2007. In preparation.

Q^2 (GeV^2)	$\frac{d\sigma}{dQ^2}$ (pb/ GeV^2)	δ_{stat} (pb/ GeV^2)	δ_{syst} (pb/ GeV^2)	δ_{ES} (pb/ GeV^2)	C_{QED}	C_{had}
10 - 15	66.0	0.8	$^{+3.7}_{-4.4}$	$^{+5.7}_{-5.9}$	0.984	0.866
15 - 20	41.4	0.6	$^{+2.0}_{-2.4}$	$^{+3.5}_{-3.6}$	0.968	0.870
20 - 30	26.2	0.3	$^{+1.0}_{-0.8}$	$^{+2.2}_{-2.0}$	0.965	0.876
30 - 50	14.0	0.1	$^{+0.4}_{-0.3}$	$^{+1.0}_{-1.1}$	0.955	0.884
50 - 100	5.82	0.06	$^{+0.17}_{-0.16}$	$^{+0.38}_{-0.38}$	0.952	0.887

Table 1: *The inclusive dijet cross sections as functions of Q^2. Included are the statistical, systematic, and jet energy scale uncertainties in columns 3, 4, and 5, respectively. Column 6 shows the correction factor from QED radiative effects applied to the measured cross sections, and column 7 shows the hadronization correction applied to the* NLOJET *calculations shown in the figures.*

$x_{\mathrm{Bj}} \times 10^{-4}$	$\frac{d\sigma}{dx_{\mathrm{Bj}}}$ (pb, $\times 10^{-4}$)	δ_{stat} (pb, $\times 10^{-4}$)	δ_{syst} (pb, $\times 10^{-4}$)	δ_{ES} (pb, $\times 10^{-4}$)	C_{QED}	C_{had}
1.7 - 3.0	85.3	1.7	$^{+5.6}_{-6.8}$	$^{+7.0}_{-6.3}$	0.987	0.910
3.0 - 5.0	113.8	1.5	$^{+5.9}_{-6.2}$	$^{+8.8}_{-8.9}$	0.975	0.887
5.0 - 10.0	83.1	0.8	$^{+3.3}_{-3.7}$	$^{+6.9}_{-7.1}$	0.969	0.876
10.0 - 25.0	29.5	0.3	$^{+0.8}_{-0.8}$	$^{+2.2}_{-2.2}$	0.958	0.876
25.0 - 100.0	2.31	0.03	$^{+0.08}_{-0.07}$	$^{+0.17}_{-0.17}$	0.948	0.862

Table 2: *The inclusive dijet cross sections as functions of x_{Bj}. Other details as in the caption to Table 1.*

Q^2 (GeV^2)	$\frac{d\sigma}{dQ^2}$ (pb/ GeV^2)	δ_{stat} (pb/ GeV^2)	δ_{syst} (pb/ GeV^2)	δ_{ES} (pb/ GeV^2)	C_{QED}	C_{had}
10 - 15	7.9	0.2	$^{+1.1}_{-1.3}$	$^{+1.0}_{-1.0}$	0.991	0.759
15 - 20	4.40	0.17	$^{+0.46}_{-0.66}$	$^{+0.45}_{-0.52}$	0.946	0.776
20 - 30	3.19	0.11	$^{+0.27}_{-0.37}$	$^{+0.38}_{-0.38}$	0.969	0.786
30 - 50	1.68	0.06	$^{+0.13}_{-0.11}$	$^{+0.20}_{-0.19}$	0.949	0.794
50 - 100	0.719	0.024	$^{+0.044}_{-0.027}$	$^{+0.077}_{-0.070}$	0.956	0.795

Table 3: *The inclusive trijet cross sections as functions of Q^2. Other details as in the caption to Table 1.*

$x_{\mathrm{Bj}} \times 10^{-4}$	$\frac{d\sigma}{dx_{\mathrm{Bj}}}$ (pb, $\times 10^{-4}$)	δ_{stat} (pb, $\times 10^{-4}$)	δ_{syst} (pb, $\times 10^{-4}$)	δ_{ES} (pb, $\times 10^{-4}$)	C_{QED}	C_{had}
1.7 - 3.0	14.7	0.7	$^{+1.5}_{-3.3}$	$^{+1.5}_{-1.9}$	1.00	0.811
3.0 - 5.0	15.9	0.5	$^{+2.0}_{-2.3}$	$^{+1.9}_{-1.8}$	0.968	0.796
5.0 - 10.0	9.6	0.3	$^{+0.9}_{-0.9}$	$^{+1.1}_{-1.1}$	0.961	0.780
10.0 - 25.0	3.35	0.10	$^{+0.21}_{-0.19}$	$^{+0.40}_{-0.37}$	0.954	0.785
25.0 - 100.0	0.192	0.013	$^{+0.032}_{-0.020}$	$^{+0.023}_{-0.022}$	0.95	0.739

Table 4: *The inclusive trijet cross sections as functions of x_{Bj}. Other details as in the caption to Table 1.*

Variable	Bin	Boundaries
$\Delta E_{T,\mathrm{HCM}}^{\mathrm{jet1,2}}$	1	$0-4$ GeV
	2	$4-10$ GeV
	3	$10-18$ GeV
	4	$18-100$ GeV
$\lvert\Sigma\vec{p}_{T,\mathrm{HCM}}^{\mathrm{jet1,2}}\rvert$	1	$0-4$ GeV
	2	$4-10$ GeV
	3	$10-16$ GeV
	4	$16-100$ GeV
$\lvert\Delta\vec{p}_{T,\mathrm{HCM}}^{\mathrm{jet1,2}}\rvert/2E_{T,\mathrm{HCM}}^{\mathrm{jet1}}$	1	$0-0.5$
	2	$0.5-0.7$
	3	$0.7-0.85$
	4	$0.85-1$
$\lvert\Delta\phi_{\mathrm{HCM}}^{\mathrm{jet1,2}}\rvert$	1	$0-\pi/4$
	2	$\pi/4-\pi/2$
	3	$\pi/2-3\pi/4$
	4	$3\pi/4-\pi$

Table 5: *The bin edges used for the measurements of the jet correlations presented. For the trijet sample, the first two bins in* $\lvert\Delta\phi_{\mathrm{HCM}}^{\mathrm{jet1,2}}\rvert$ *are combined.*

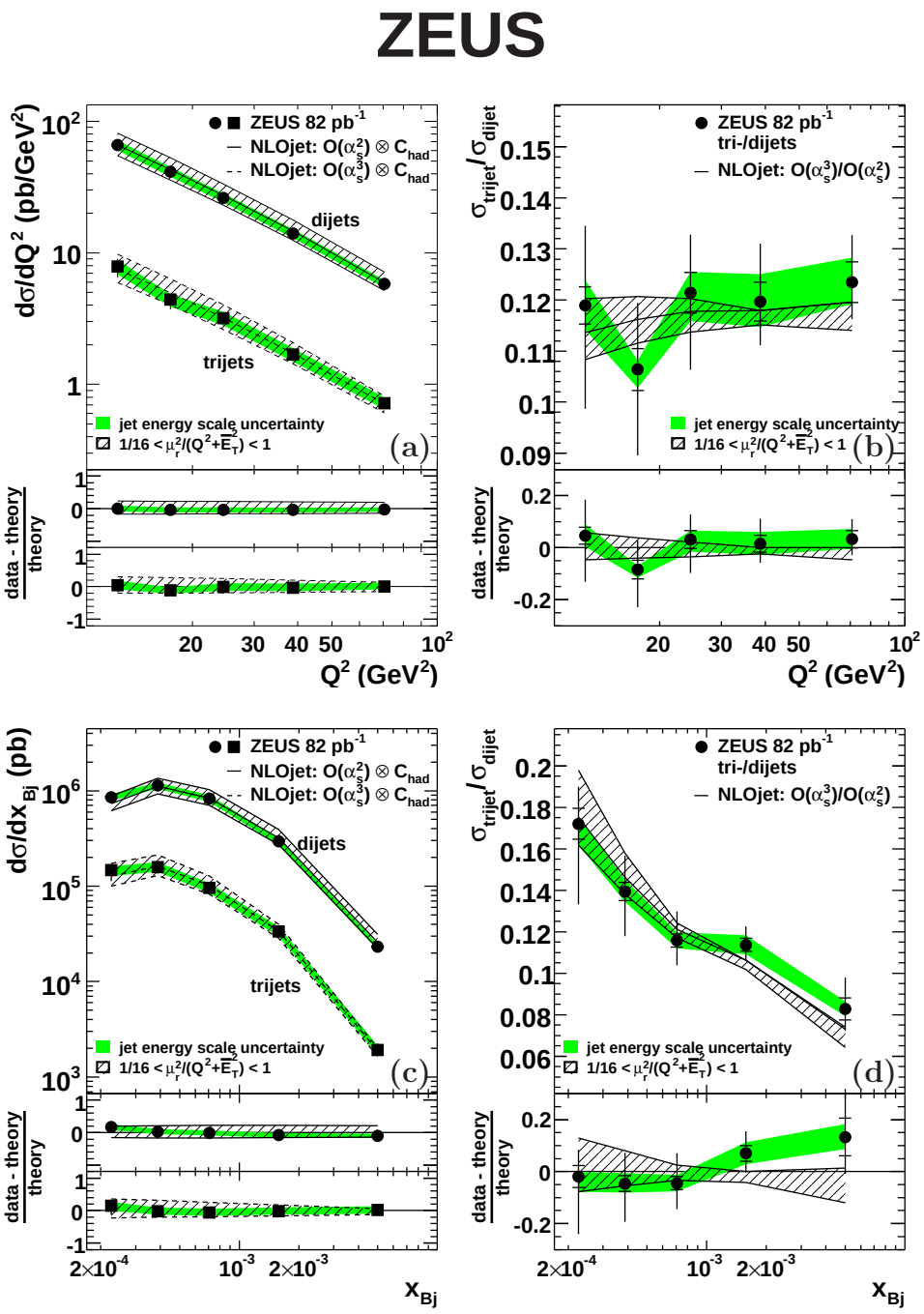

Figure 1: *Inclusive dijet and trijet cross sections as functions of (a) Q^2 and (c) x_{Bj}. Figures (b) and (d) show the ratios of the trijet to dijet cross sections. The bin-averaged differential cross sections are plotted at the bin centers. The inner error bars represent the statistical uncertainties. The outer error bars represent the quadratic sum of statistical and systematic uncertainties not associated with the jet energy scale. The shaded band indicates the jet energy scale uncertainty. The predictions of perturbative QCD at NLO, corrected for hadronisation effects and using the CTEQ6 parameterisations of the proton PDFs, are compared to data. The lower parts of the plots show the relative difference between the data and the corresponding theoretical prediction. The hatched band represents the renormalisation-scale uncertainty of the QCD calculation.*

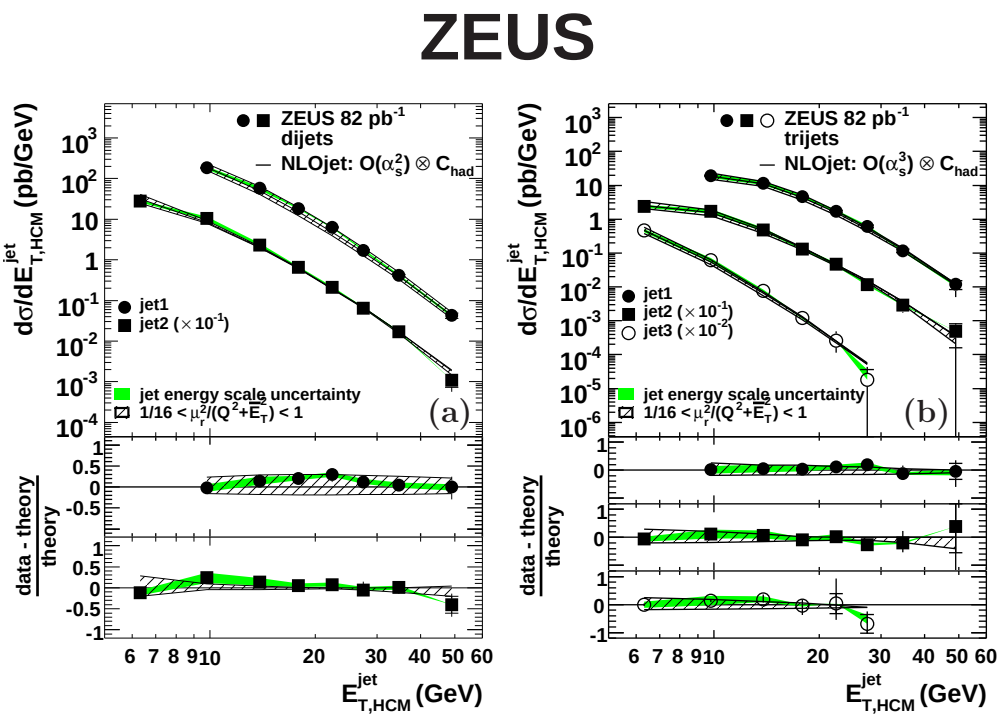

Figure 2: *Inclusive dijet (a) and trijet (b) cross sections as functions of* $E^{\rm jet}_{T,\rm HCM}$ *with the jets ordered in* $E^{\rm jet}_{T,\rm HCM}$. *The cross sections of the second and third jet were scaled for readability. Other details as in the caption to Fig. 1.*

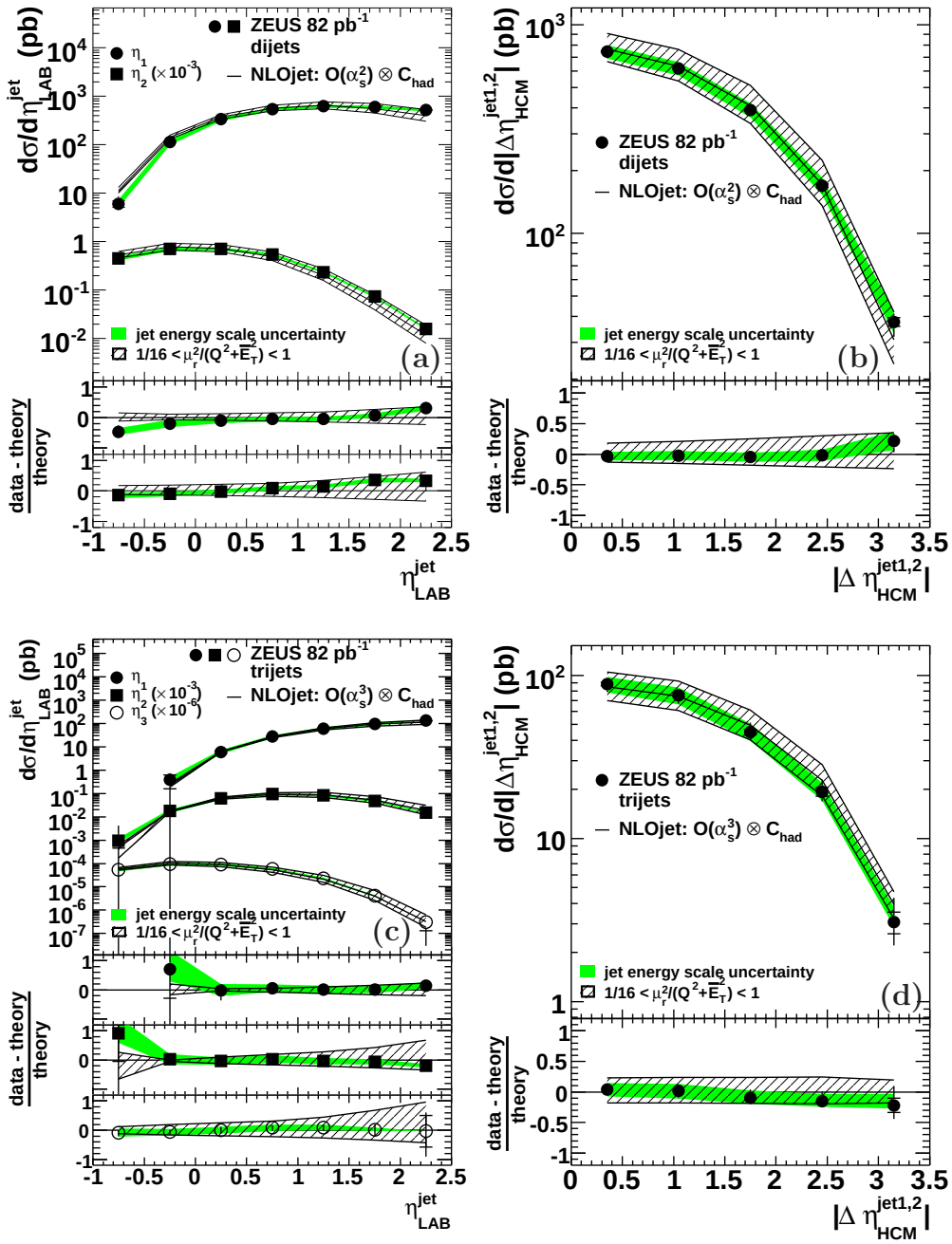

Figure 3: *The inclusive dijet (a) and trijet (c) cross sections as functions of* $\eta^{\rm jet}_{\rm LAB}$ *with the jets ordered in* $\eta^{\rm jet}_{\rm LAB}$*:* $\eta^{\rm jet1}_{\rm LAB} > \eta^{\rm jet2}_{\rm LAB} > \eta^{\rm jet3}_{\rm LAB}$*. The cross sections of the second and third jet were scaled for readability. Figures (b) and (d) show the dijet and trijet cross sections as functions of* $|\Delta\eta^{\rm jet1,2}_{\rm HCM}|$ *between the two jets with highest* $E^{\rm jet}_{T,\rm HCM}$*. Other details as in the caption in Fig. 1.*

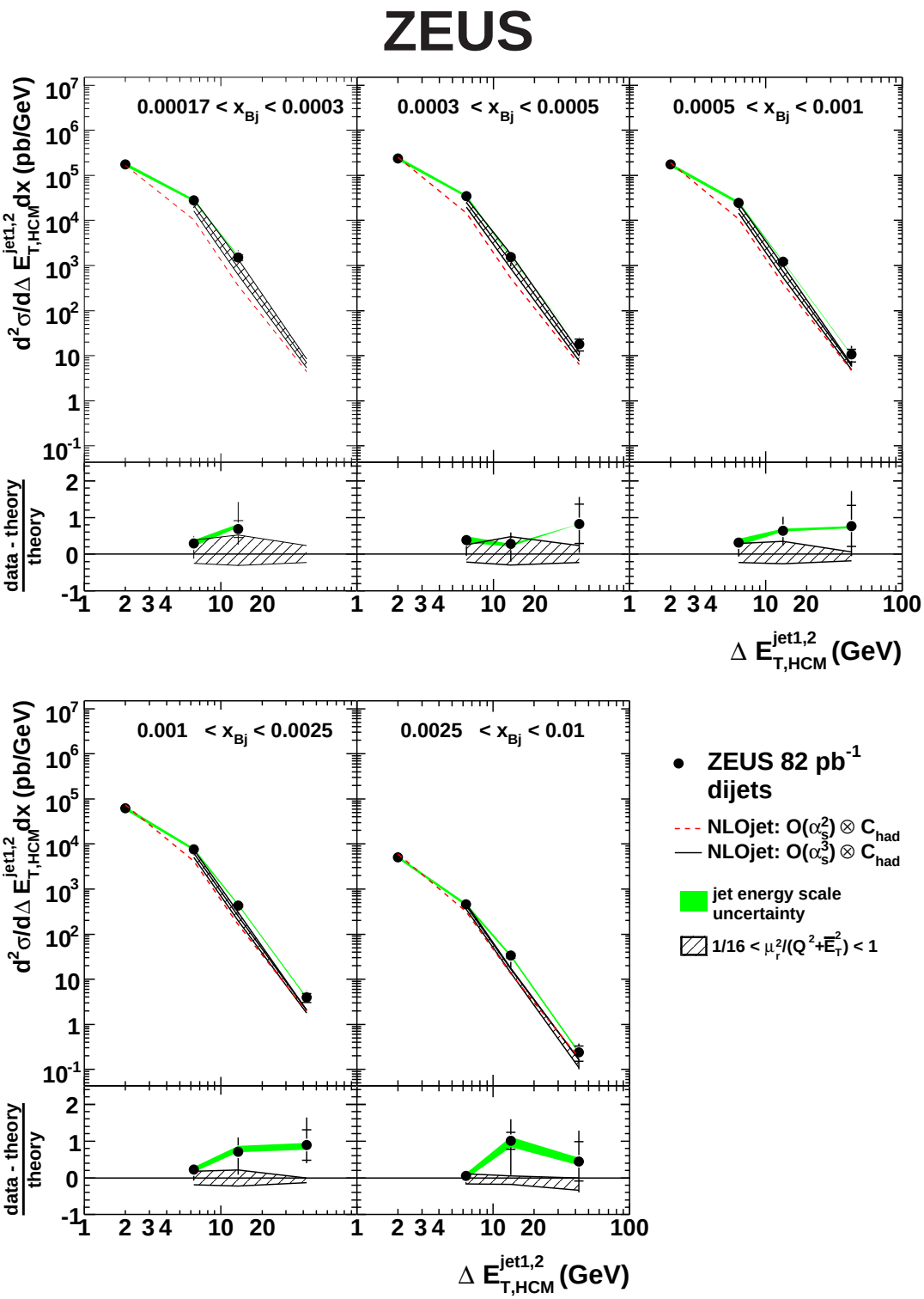

Figure 4: *Dijet cross sections as functions of* $\Delta E_{T,\mathrm{HCM}}^{\mathrm{jet1,2}}$. *The* NLOJET *calculations at* $\mathcal{O}(\alpha_s^2)$ ($\mathcal{O}(\alpha_s^3)$) *are shown as dashed (solid) lines. The lower parts of the plots show the relative difference between the data and the* $\mathcal{O}(\alpha_s^3)$ *predictions. The boundaries for the bins in* $\Delta E_{T,\mathrm{HCM}}^{\mathrm{jet1,2}}$ *are given in Table 5. Other details as in the caption to Fig. 1.*

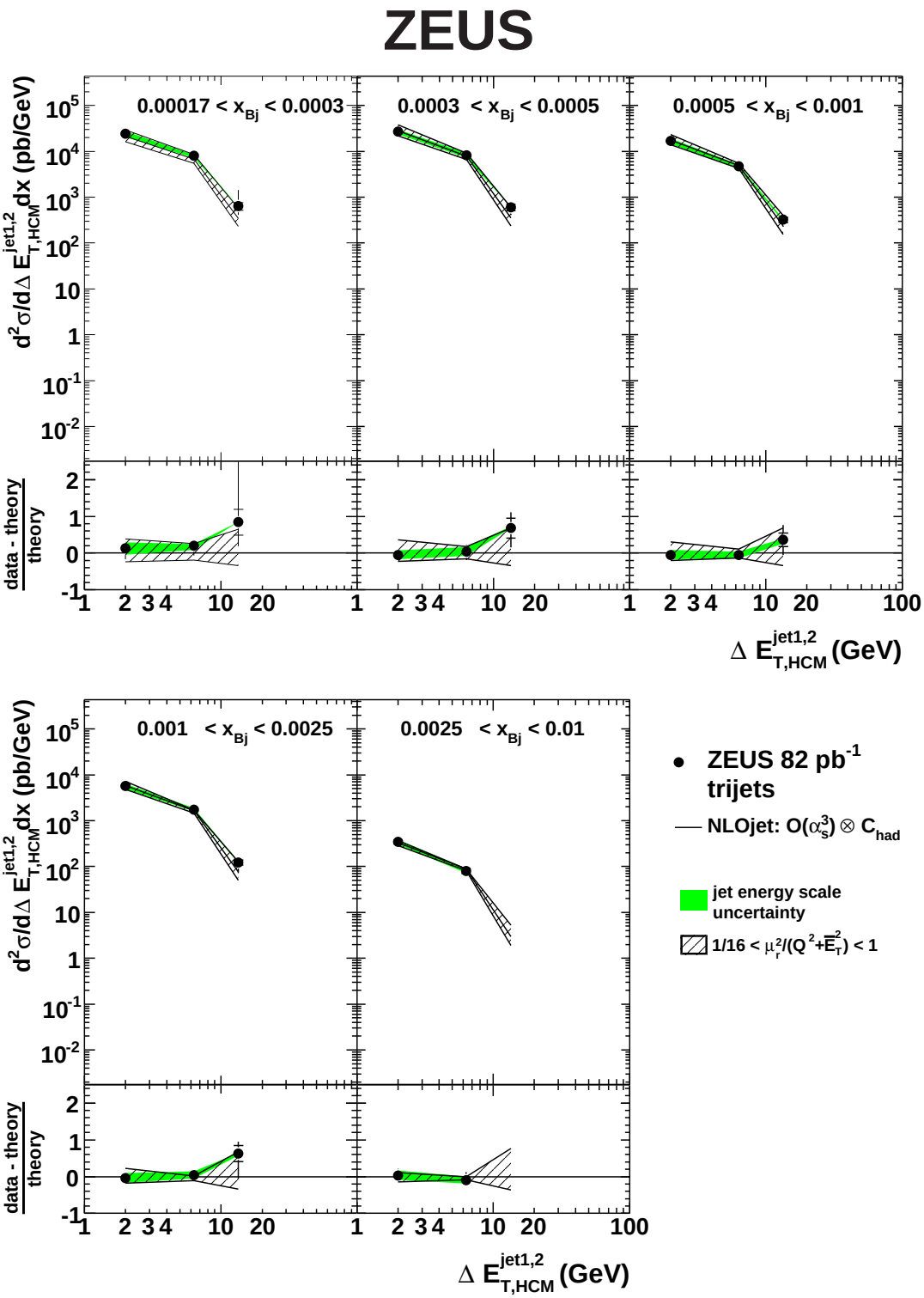

Figure 5: *Trijet cross sections as functions of* $\Delta E^{\mathrm{jet1,2}}_{T,\mathrm{HCM}}$. *The measurements are compared to* NLOJET *calculations at* $\mathcal{O}(\alpha_s^3)$. *The boundaries for the bins in* $\Delta E^{\mathrm{jet1,2}}_{T,\mathrm{HCM}}$ *are given in Table 5. Other details as in the caption to Fig. 1.*

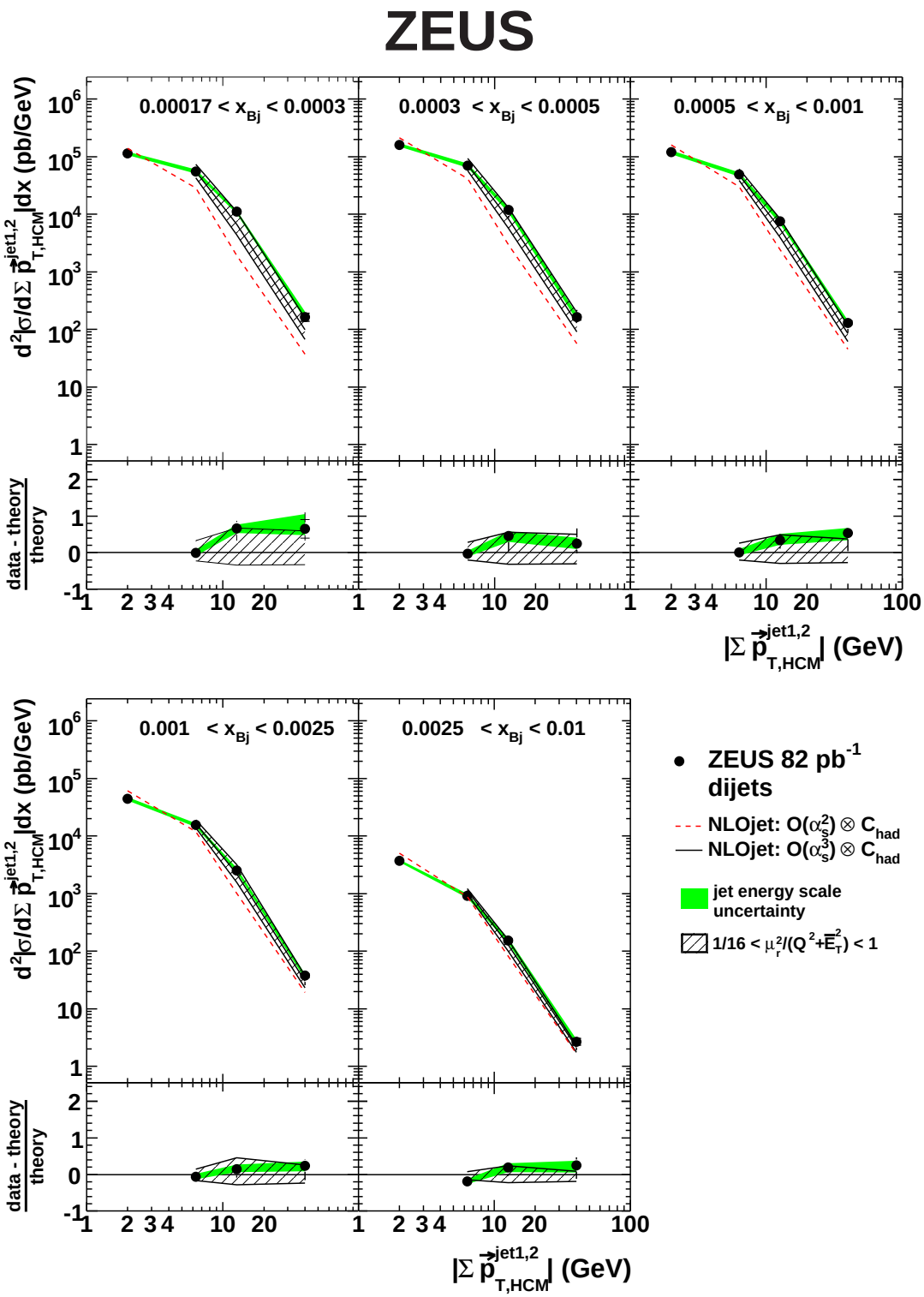

Figure 6: *Dijet cross sections as functions of* $|\Sigma\vec{p}_{T,\mathrm{HCM}}^{\,\mathrm{jet1,2}}|$. *The* NLOJET *calculations at* $\mathcal{O}(\alpha_s^2)$ ($\mathcal{O}(\alpha_s^3)$) *are shown as dashed (solid) lines. The lower parts of the plots show the relative difference between the data and the* $\mathcal{O}(\alpha_s^3)$ *predictions. The boundaries for the bins in* $|\Sigma\vec{p}_{T,\mathrm{HCM}}^{\,\mathrm{jet1,2}}|$ *are given in Table 5. Other details as in the caption to Fig. 1.*

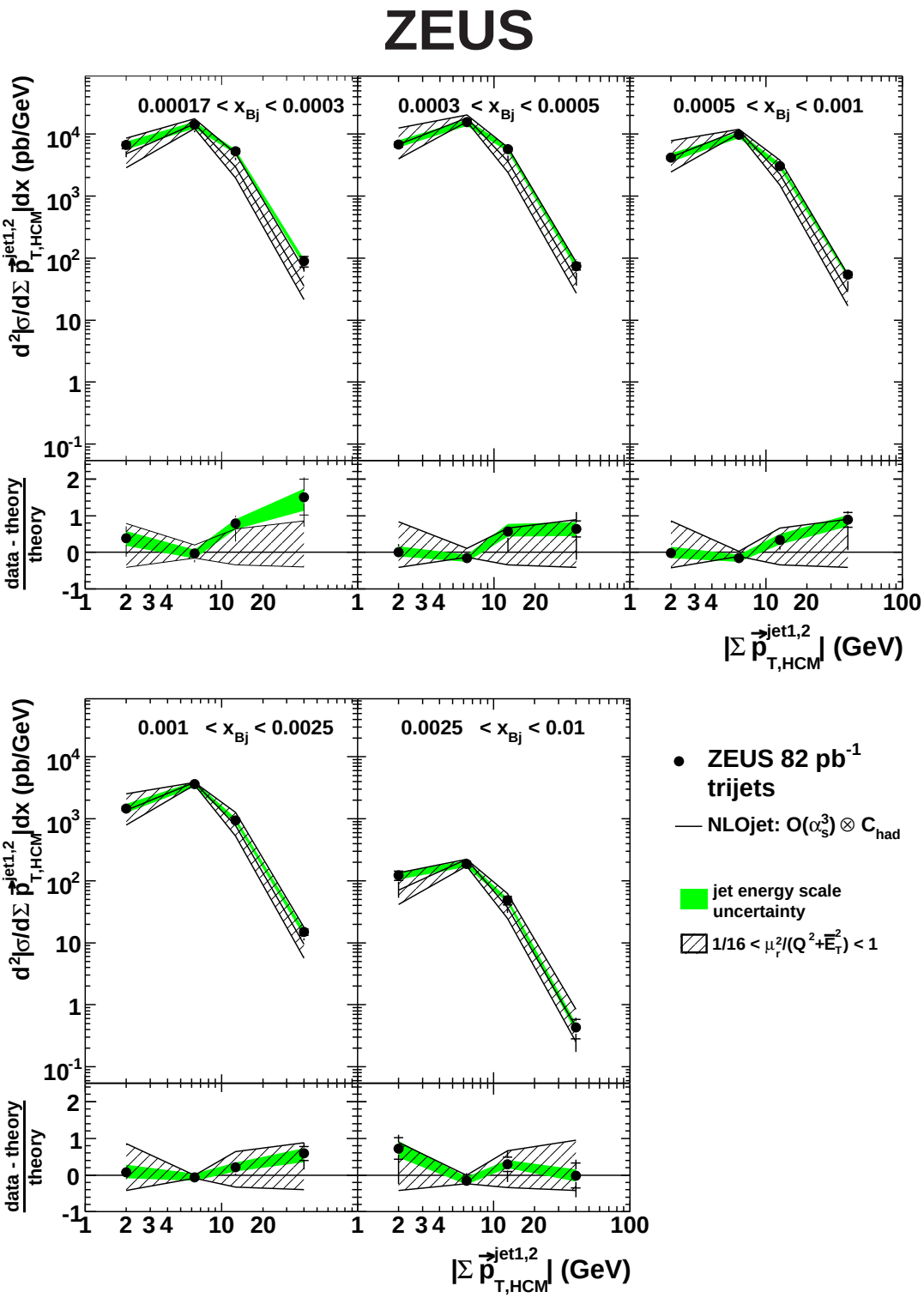

Figure 7: *Trijet cross sections as functions of* $|\Sigma\vec{p}^{\,\mathrm{jet1,2}}_{T,\mathrm{HCM}}|$. *The measurements are compared to* NLOJET *calculations at* $\mathcal{O}(\alpha_s^3)$. *The boundaries for the bins in* $|\Sigma\vec{p}^{\,\mathrm{jet1,2}}_{T,\mathrm{HCM}}|$ *are given in Table 5. Other details as in the caption to Fig. 1.*

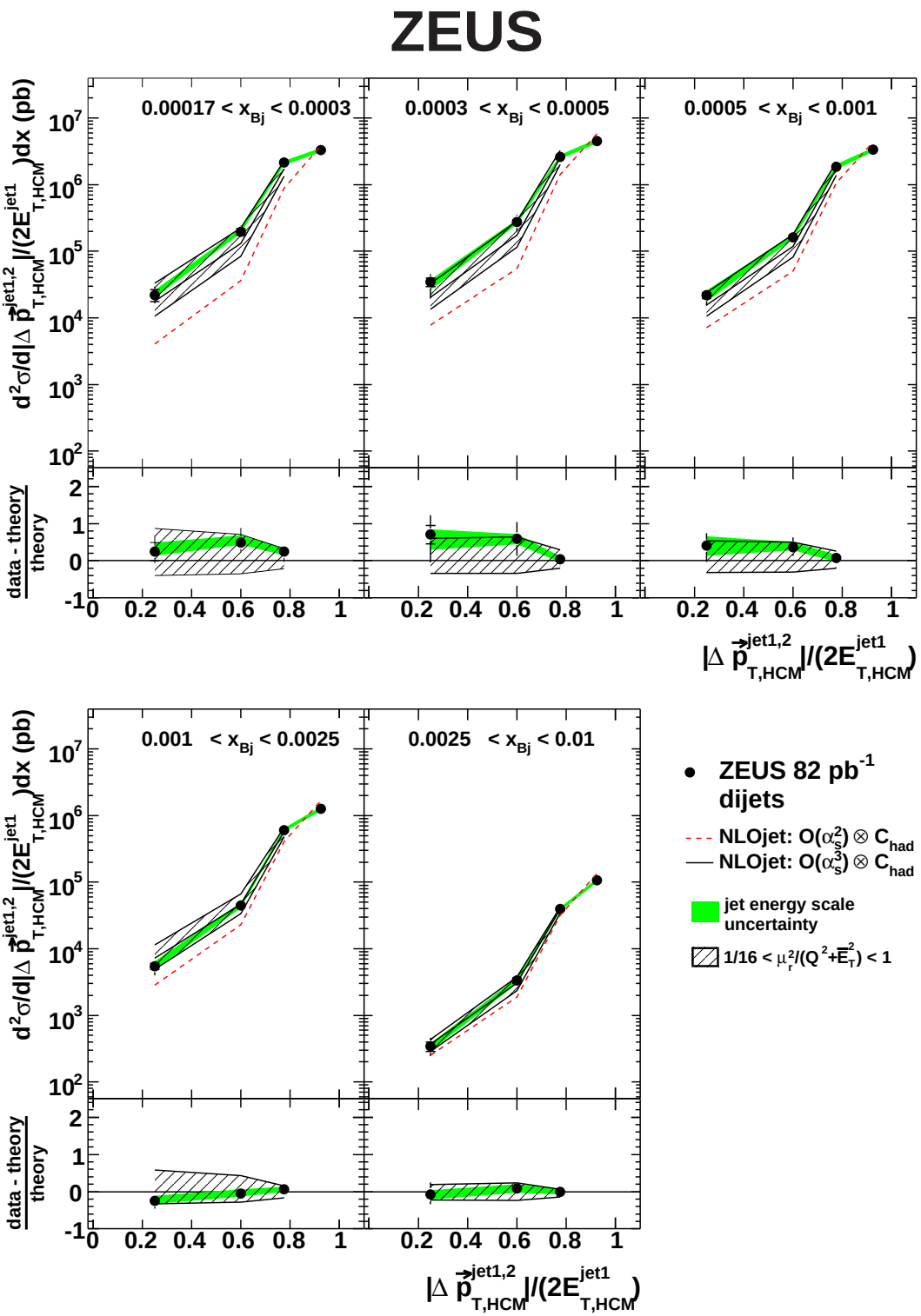

Figure 8: *Dijet cross sections as functions of* $|\Delta\vec{p}^{\,\mathrm{jet1,2}}_{T,\mathrm{HCM}}|/(2E^{\mathrm{jet1}}_{T,\mathrm{HCM}})$. *The* NLOJET *calculations at* $\mathcal{O}(\alpha_s^2)$ ($\mathcal{O}(\alpha_s^3)$) *are shown as dashed (solid) lines. The lower parts of the plots show the relative difference between the data and the* $\mathcal{O}(\alpha_s^3)$ *predictions. The boundaries for the bins in* $|\Delta\vec{p}^{\,\mathrm{jet1,2}}_{T,\mathrm{HCM}}|/(2E^{\mathrm{jet1}}_{T,\mathrm{HCM}})$ *are given in Table 5. Other details as in the caption to Fig. 1.*

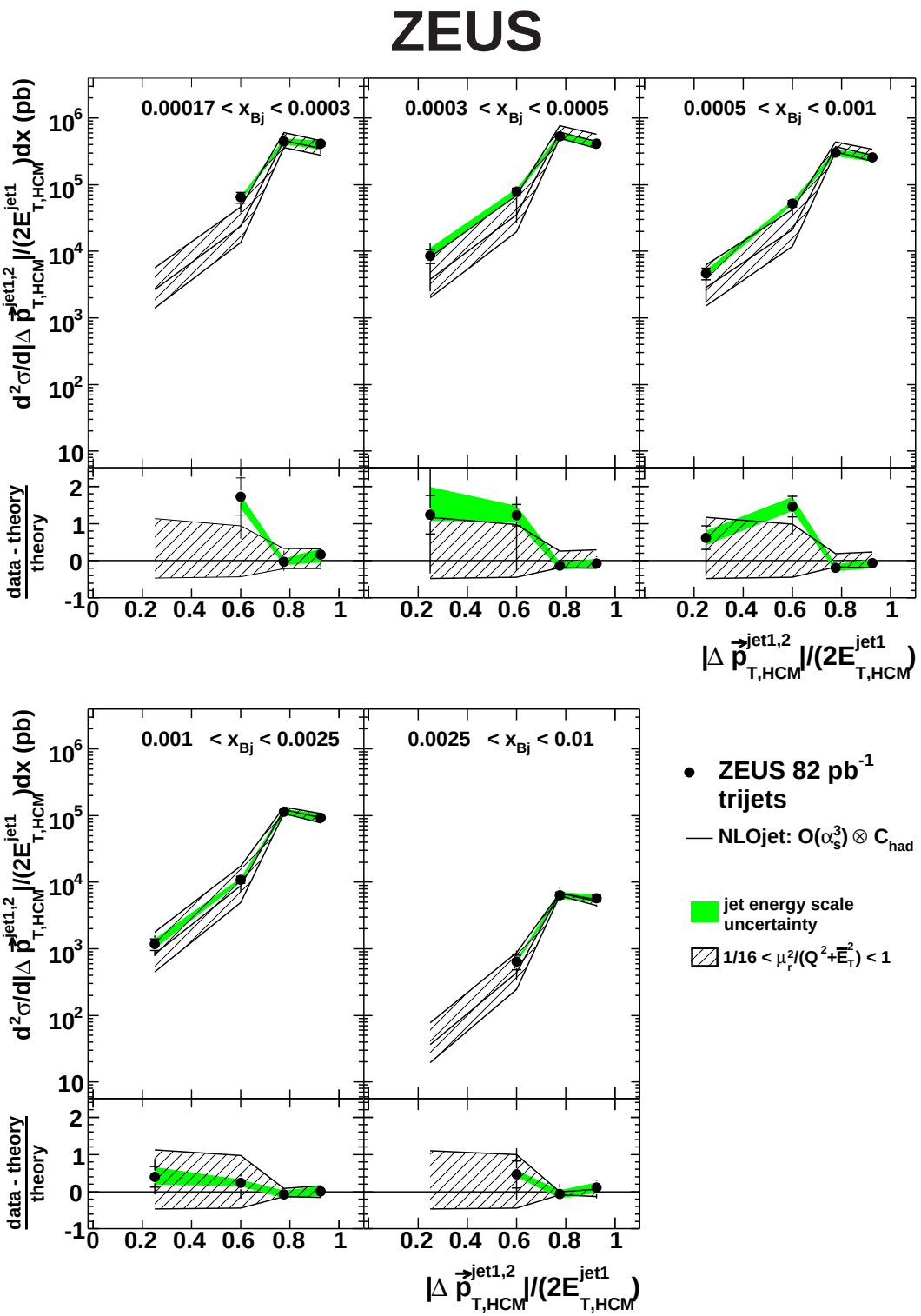

Figure 9: *Trijet cross sections as functions of* $|\Delta\vec{p}^{\,\mathrm{jet1,2}}_{T,\mathrm{HCM}}|/(2E^{\mathrm{jet1}}_{T,\mathrm{HCM}})$. *The measurements are compared to* NLOJET *calculations at* $\mathcal{O}(\alpha_s^3)$. *The boundaries for the bins in* $|\Delta\vec{p}^{\,\mathrm{jet1,2}}_{T,\mathrm{HCM}}|/(2E^{\mathrm{jet1}}_{T,\mathrm{HCM}})$ *are given in Table 5. Other details as in the caption to Fig. 1.*

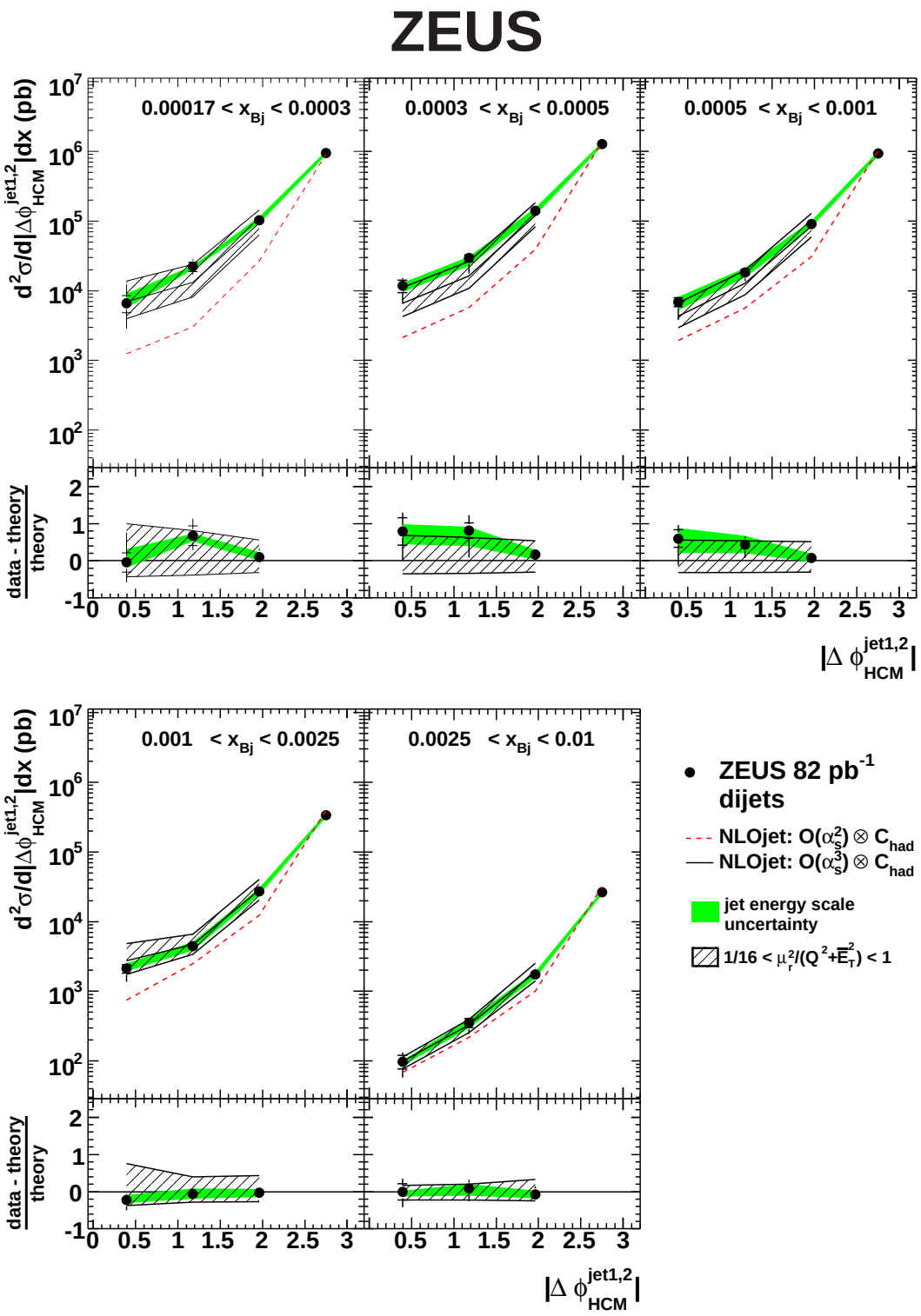

Figure 10: *Dijet cross sections as functions of* $|\Delta\phi^{\rm jet1,2}_{\rm HCM}|$. *The* NLOJET *calculations at* $\mathcal{O}(\alpha_s^2)$ ($\mathcal{O}(\alpha_s^3)$) *are shown as dashed (solid) lines. The lower parts of the plots show the relative difference between the data and the* $\mathcal{O}(\alpha_s^3)$ *predictions. The boundaries for the bins in* $|\Delta\phi^{\rm jet1,2}_{\rm HCM}|$ *are given in Table 5. Other details as in the caption to Fig. 1.*

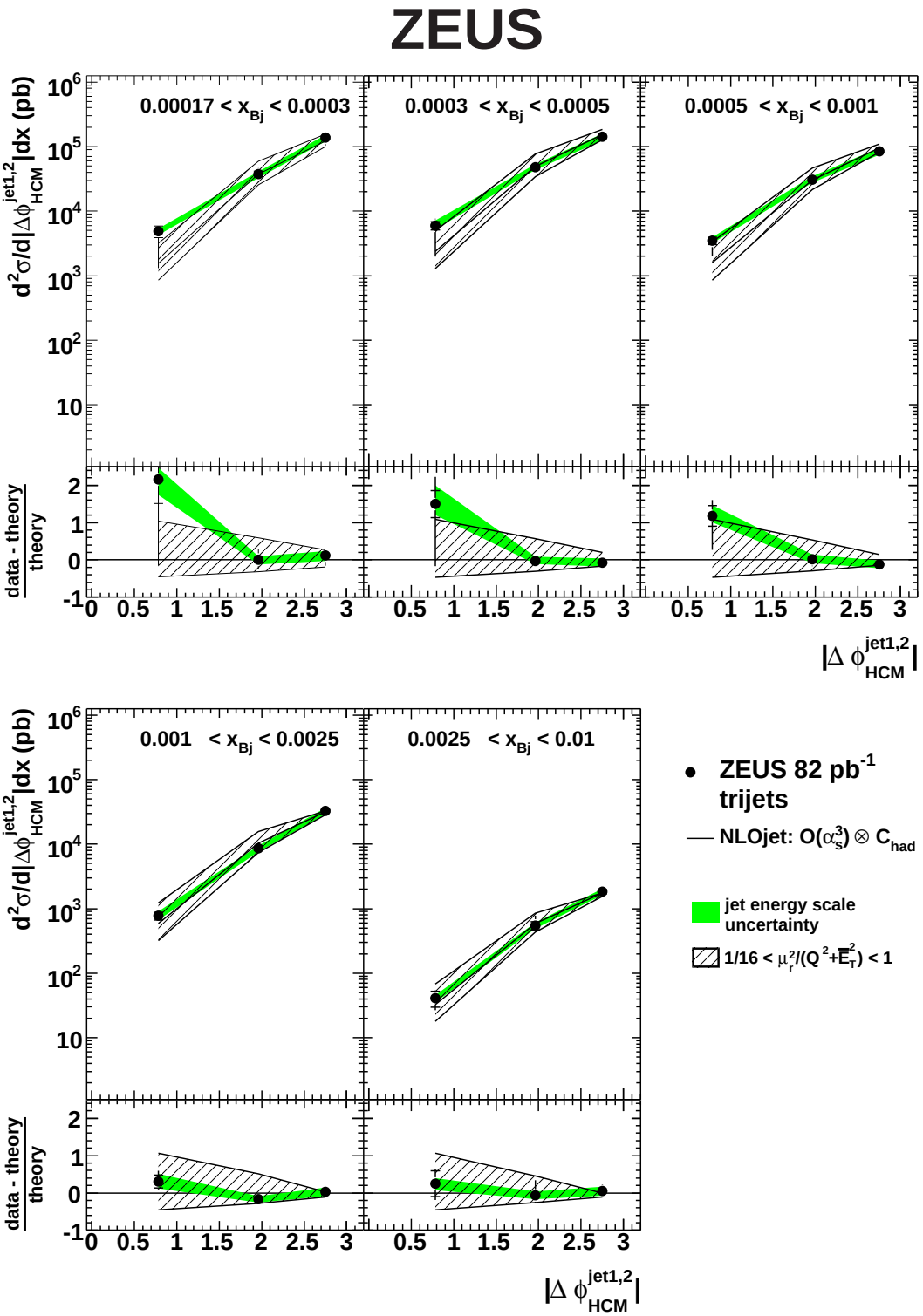

Figure 11: *Trijet cross sections as functions of* $|\Delta\phi^{\mathrm{jet1,2}}_{\mathrm{HCM}}|$. *The measurements are compared to* NLOJET *calculations at* $\mathcal{O}(\alpha_s^3)$. *The boundaries for the bins in* $|\Delta\phi^{\mathrm{jet1,2}}_{\mathrm{HCM}}|$ *are given in Table 5. Other details as in the caption to Fig. 1.*

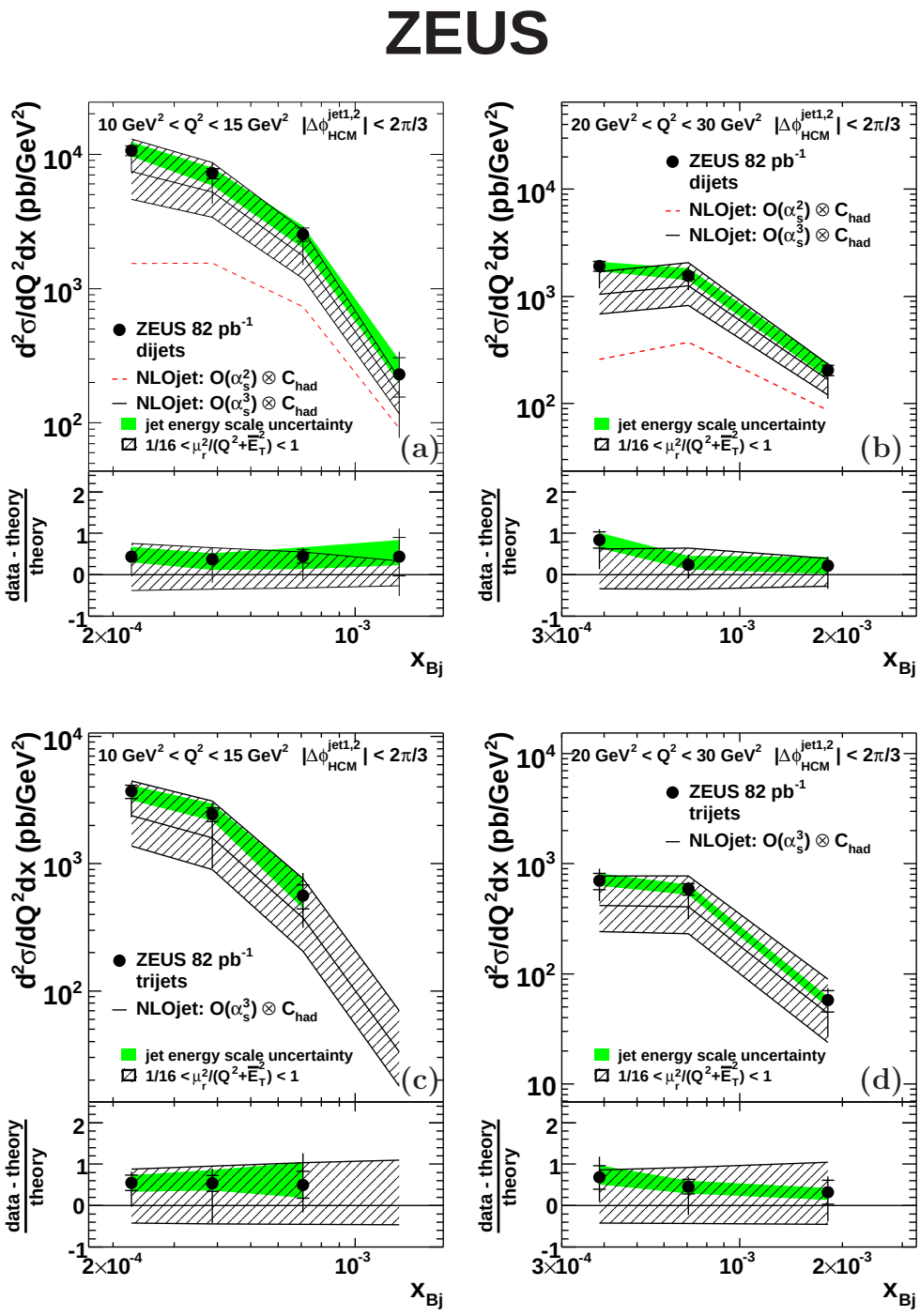

Figure 12: *The dijet and trijet cross sections for events with* $|\Delta\phi^{\mathrm{jet1,2}}_{\mathrm{HCM}}| < 2\pi/3$ *as functions of* x_{Bj} *in two different* Q^2*-bins. The* NLOJET *calculations at* $\mathcal{O}(\alpha_s^2)$ $(\mathcal{O}(\alpha_s^3))$ *are shown as dashed (solid) lines. The trijet measurements are compared to* NLOJET *calculations at* $\mathcal{O}(\alpha_s^3)$*. The lower parts of the plots in (a) and (b) show the relative difference between the data and the* $\mathcal{O}(\alpha_s^3)$ *predictions. Other details as in the caption to Fig. 1.*